small methods
www.small-methods.com

Boosting ORR/OER Activity of Graphdiyne by Simple Heteroatom Doping

Jinxing Gu, Saneliswa Magagula, Jingxiang Zhao, and Zhongfang Chen**

Nitrogen-doped graphdiynes recently emerged as promising metal-free oxygen reduction reaction (ORR) electrocatalysts. However, which type of N-dopants contributing to the enhanced catalytic performance and the catalytic performances of other heteroatom-doped graphdiynes has not been explored systematically. Herein, ORR and oxygen evolution reaction (OER) catalytic performances of X-doped graphdiynes are examined by means of DFT computations (X = B, N, P, and S). It is revealed that the graphitic S-doped graphdiyne (Model S1), the sp-N-doped graphdiyne (Model N3) and the graphitic P-doped graphdiyne (Model P1) exhibit comparable or even better ORR/OER activities than Pt/C or RuO_2, with ORR activity trend as Model S1 > Pt/C > Model N3 and OER trend as Model P1 > RuO_2 > Model N3. The carbon atoms near N- and S-dopants and featuring large positive charge are the ORR active sites in Models N3 and S1, whereas the carbon atoms near N- and P-dopants and possessing high spin are the OER active sites in Models N3 and P1. Overall, this study not only gains deep insights into the catalytic activity of N-doped graphdiyne for ORR, but also guides developing of graphdiyne-based ORR/OER catalysts beyond N-doping.

1. Introduction

Fuel cells,[1,2] rechargeable metal–air batteries,[3,4] and water splitting[5,6] technologies provide a promising blueprint for sustainable and renewable energy supplies.[7] To realize these technologies, two sluggish chemical reactions are at the core: oxygen reduction reaction (ORR) and oxygen evolution reaction (OER). Currently, the industrially used ORR catalysts are Pt/C, while the best OER catalysts are oxides of Ir and Ru.[8] These noble metal-based catalysts are limited in commercialization due to their high cost and other drawbacks. For example, Pt/C suffers from voltage-dependent area loss,[9] poor methanol tolerance, and CO poisoning.[10] Therefore, it is critical and desirable to search for durable, active, and inexpensive catalysts. Several strategies, such as reducing the precious metal loading,[11] developing single-atom catalysts and nonprecious metal catalysts,[12–18] and fabricating metal-free catalysts[19] have been exploited. Among these strategies, metal-free catalysts with controllable compositions are quite attractive because of their low-cost, high stability, and high efficiency.[19–24]

Graphene, a 2D material first fabricated in 2004,[25] has many unique properties, such as large surface area and high conductivity. Graphene-based nanomaterials are among the most widely studied ORR metal-free catalysts. Notably, the catalytic performance can be enhanced by doping with various heteroatoms such as N, B, P, and S;[26–28] these heteroatoms influence the activity of graphene by changing the bandgap, spin, and charge distributions.[29] For example, compared with commercially available Pt/C, doping nitrogen endows graphene with better activity and stability and reduces the crossover and poison effect for ORR in alkaline media.[30] In addition, nitrogen-doped graphene materials can even act as ORR/OER bifunctional metal-free catalysts,[31] which are highly desirable for rechargeable metal–air batteries.[32]

Inspired by graphene, other 2D materials have been explored as ORR/OER catalysts, such as phosphorene,[33] antimonene,[34] and graphitic carbon nitride ($g\text{-}C_3N_4$).[35] Understanding the influence of doped heteroatoms to these 2D materials at the atomic level can greatly facilitate catalyst design. As demonstrated by Pei et al.,[36] for instance, the S-doped $g\text{-}C_3N_4$ as a bifunctional catalyst (for oxygen reduction and hydrogen evolution reactions) affords superior reaction kinetics relative to its B- or P-doped counterpart.

An analogue of graphene is graphdiyne: a semiconductor that consists of carbon hexagonal rings (sp^2-hybridized C) and diacetylenic linkages (−C≡C−C≡C−, sp-hybridized C).[37–39] Recently, N-doped graphdiynes emerged as promising ORR metal-free catalysts, with low overpotential, small crossover effect, and long-term stability.[40–42] For example, Liu et al.[43] prepared N-doped graphdiyne by heating graphdiyne under high-purity ammonia mixed with argon. The as-prepared N-doped graphdiyne showed high ORR activity ($E_{onset} \approx 0.899$ V vs RHE) and good tolerance to methanol in alkaline media. Notably, doping nitrogen to graphdiyne could introduce two

J. Gu, S. Magagula, Prof. Z. Chen
Department of Chemistry
University of Puerto Rico
Rio Piedras Campus, San Juan, Puerto Rico 00931, USA
E-mail: zhongfangchen@gmail.com
Prof. J. Zhao
College of Chemistry and Chemical Engineering
Key Laboratory of Photoelectronic Bandgap Materials
Harbin Normal University
Ministry of Education
Harbin 150025, China
E-mail: xjz_hmily@163.com
The ORCID identification number(s) for the author(s) of this article can be found under https://doi.org/10.1002/smtd.201800550.

DOI: 10.1002/smtd.201800550

kinds of dopants: sp^2-N and sp-N, depending on which hybridized carbon is substituted.[44] Substituting sp^2-C yields sp^2-N dopants, namely graphitic N and pyridinic N,[46] while substituting sp-C yields sp-N dopants, in the form of $-\overset{+}{N}\equiv C-C\equiv C-$ and $-C\equiv\overset{+}{N}-C\equiv C-$.[44] Both the sp^2-N (pyridinic N) and the sp-N dopants are believed to help promote the ORR performance of graphdiynes.[45–47] However, Liu et al.[43] proposed that the sp-N dopants plays a more important role than sp^2-N on the basis of the calculated charge distribution and O_2 adsorption energies. Moreover, Zhang et al. successfully realized N and F codoped graphdiyne, which exhibited very good activity toward ORR as indicated by its onset potential of 1.0 V versus RHE.[48] In the same work, graphdiynes doped solely by B, S, and F were also fabricated, but their catalytic performances were not reported yet.[48] On the theoretical side, several studies have investigated the electronic structure and ORR catalytic performance of B and N doped graphdiynes, which promotes the design of graphdiyne-based electrocatalysts.[49–51]

However, to our best knowledge, the ORR performance of only a few doped graphdiynes (B and N) has been examined, while no efforts toward OER activity of doped graphdiynes have been made so far. Thus, several issues are yet to be addressed to develop graphdiyne-based ORR/OER electrocatalysts: Where are the actual active sites located? Which N doping type is essential to ORR? Can N and other heteroatom (e.g., B, P, and S)-doped graphdiynes exhibit good activities toward ORR and/or OER? In the present work, we comprehensively studied the electrocatalytic activities of N, B, P, and S-doped graphdiyne toward ORR/OER by means of density functional theory (DFT) computations. Our calculations revealed that the sp-N doped graphdiyne with a specific doping style ($-C\equiv\overset{+}{N}-C\equiv C-$) exhibits the best activity for both ORR and OER among N-doped graphdiynes. We also demonstrated that the graphitic S-doped graphdiyne exhibits the best catalytic activity toward ORR, and the graphitic P-doped graphdiyne has the best catalytic activity toward OER, among all the heteroatom (B, N, P and S)-doped graphdiynes examined in this study.

2. Computational Methods

Geometry optimizations and total energy calculations were performed by spin-polarized DFT computations using the DMol^3 package.[52] The Perdew–Burke–Ernzerhof (PBE) functional[53] within the generalized gradient approximation (GGA) was employed. We also considered van der Waals interactions following the empirical correction in Grimme's scheme,[54] and included the solvent effect using the conductor-like screen model (COSMO) where the dielectric constant for water is 78.54.[55] The double numerical plus polarization (DNP) basis set was utilized throughout this work.[56] A global orbital cutoff of 4.0 Å, an energy convergence level of 1.0×10^{-5} Ha, and an SCF tolerance of 1.0×10^{-6} Ha were adopted. All the structural models were constructed from a graphdiyne supercell ($2 \times 2 \times 1$) with corresponding lattice constants: $a = b = 18.94$ Å and $c = 15$ Å. Due to the large lattice constant, the Brillouin zone was sampled by a $2 \times 2 \times 1$ k-mesh grid via Monkhorst-Pack method,[57] and the reliability of this k-point setting was validated by test computations (Figure S1, Supporting Information). Atomic charge and spin distribution calculations were performed by the Hirshfeld method.[58]

The Gibbs reaction free energy change (ΔG) of each elementary step in ORR/OER was evaluated based on the computational hydrogen electrode (CHE) model developed by Nørskov and coworkers.[59] We denoted the free adsorption energies of O-containing intermediates in the ORR/OER four-electron pathway as ΔG(*OOH), ΔG(*O), and ΔG(*OH). These free adsorption energies were calculated using the free energies of H_2O molecule in the liquid phase and H_2 molecule in the gas phase as references. For example, Equation 1 was used to obtain ΔG(*OH)

$$H_2O(l) + * = *OH + \tfrac{1}{2}H_2(g) \quad (1a)$$

$$\Delta G(^*OH) = G(^*OH) + \tfrac{1}{2}G(H_2(g)) - G(H_2O(l)) - G(*) \quad (1b)$$

The free energy G for each species is $G = E + E_{ZPE} - TS$, where E is the total energy, E_{ZPE} is the zero-point energy, S is the entropy, and T is set to 300 K. For all species, the total energies are obtained by DFT computations. The E_{ZPE} and S values of O-containing intermediates (*O, *OH, *OOH) are calculated by keeping the substrates (i.e., doped graphdiynes) fixed, while the E_{ZPE} and S values of the H_2 molecule in the gas phase and in the liquid phase are from ref. [59]. The Gibbs free energy of the O_2 molecule is derived as $G(O_2(g)) = 2G(H_2O(l)) - 2G(H_2(g)) + 4.92$ eV, since DFT cannot very accurately calculate the energy of the triplet O_2 molecule.

3. Results and Discussions

3.1. Structures, Electronic Properties, and Stabilities of Doped Graphdiynes

To study the ORR/OER activity of heteroatom X-doped graphdiynes, we chose B, N, P, and S dopants as representatives, since they are the most widely studied dopants in the chemistry of carbon-based materials.[60] In total, 15 structural models were constructed for X-doped graphdiynes, including one model for pristine graphdiyne (Gdy), five models for N-doped graphdiynes, and three models each for B-, P- and S-doped graphdiynes, as shown in **Figure 1**. For clarity, unique carbon atoms (inside the green frameworks in Model Gdy) are labeled by numbers from 1 to 11. Due to the symmetry, substituting carbon atoms 1, 2, and 3 in Model Gdy, respectively, by heteroatom X (X = B, N, P, and S) result in three different models, namely X1, X2, and X3. Model X1 is also known as graphitic X-doped graphdiyne, as the X heteroatom replaces the sp^2-hybridized carbon atom, while X2 and X3 are sp-X-doped graphdiynes with sp-hybridized carbon atoms substituted by X atoms. Besides Models X1–3, Model pdN and Model NH_2 are constructed for representing the pyridinic N-doped and the amino group doped graphdiynes, respectively. Note that all these five N-doped graphdiynes have been obtained experimentally.[44–46] By examining these 15 models, we can find out the most crucial X dopant and the most active X-doped graphdiyne for ORR/OER.

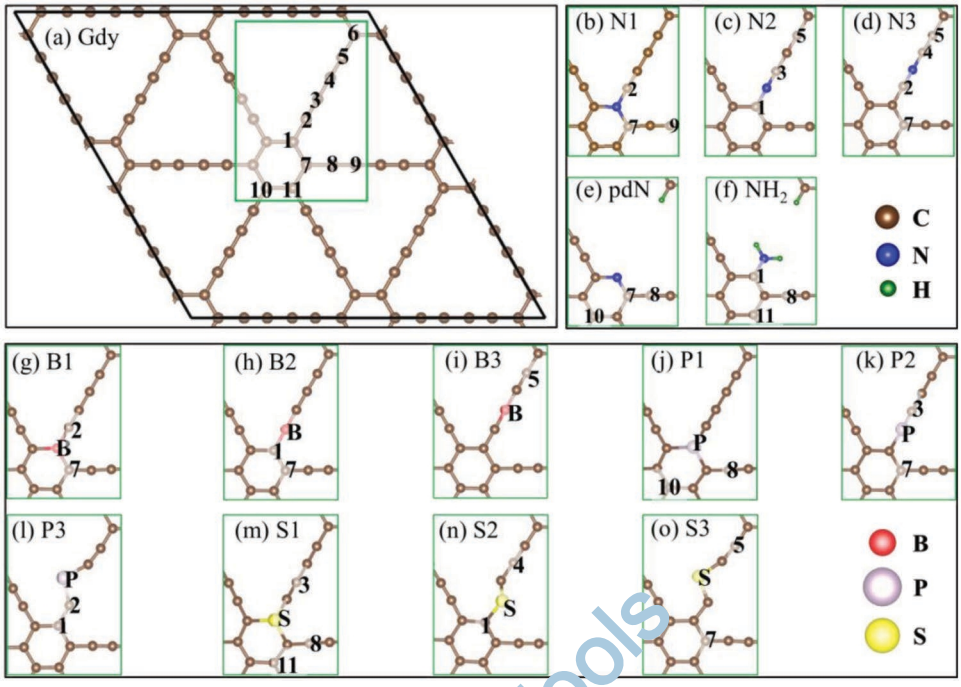

Figure 1. Constructed models for pristine, and N-, B-, P-, S-doped graphdiyne: a) pristine graphdiyne Gdy, b) N1, c) N2, d) N3, e) pdN, f) NH_2; B-doped graphdiyne: g) B1, h) B2, i) B3; P-doped graphdiyne: j) P1, k) P2, l) P3; S-doped graphdiyne: m) S1, n) S2, o) S3. Note that Model Gdy has three possible active sites (C1, C2, C3). For other models, the heteroatoms themselves, and the carbon atoms with high spin and/or charge density were considered as possible active sites (labeled according to the relative position in (a).

The pristine graphdiyne is a semiconductor with a bandgap of 0.46 eV,[38] which is reduced upon doping B, N, P, or S for all the considered models (Figure S3, Supporting Information). At a doping concentration of about 4% (atomic percentage), the B- and S-doped graphdiynes can reduce the bandgap to 0.16 and 0.28 eV, respectively; while N- and P-doped graphdiynes can even be metallic. The bandgaps of the B- and S-doped graphdiynes are further reduced at higher doping concentrations (Figure S4, Supporting Information): at a doping concentration of about 5.6% (atomic percentage), all the B-doped graphdiynes become metallic, while the bandgap of S-doped graphdiynes can be narrowed to 0.01 eV (Model S3). The reduced bandgaps are beneficial to the electron transfer when these doped graphdiynes are utilized as electrode materials.

Structurally, doping B or N atoms to graphdiynes preserves the original planar geometry, while doping P or S leads to an out-of-the-plane distortion except for Models P3 and S3 (Figure S2, Supporting Information), mostly due to the larger atomic radii of P and S atoms.

To evaluate the relative stabilities of doped graphdiynes, we computed their cohesive energies (E_{coh}) via the equation: $E_{coh} = (E_{model} - mE_C - nE_X)/(m + n)$, where E_{model} is the total energy of the examined model, E_C and E_X are the total energies of isolated C and heteroatom X, while m and n are the number of C and X atoms in the cell. According to our definition, a more negative cohesive energy indicates increased thermodynamic stability of the corresponding model. All these doped graphdiynes have rather negative cohesive energies, indicating their high thermodynamic stabilities. Based on the cohesive energies (**Figure 2**a), N, P and S dopants prefer the X2 doping style, while B dopant prefers X1.

The thermodynamically preferred doping configurations can be explained by the electronic effects. The graphitic S-doped graphdiyne (Model S1) features a sp^3-hybridized S atom, as revealed by the natural bond orbital (NBO)[61] analysis; the classic tetrahedral characteristic of sp^3-hybridization gives rise to the geometric distortion, which destroys the aromaticity of the hexagonal ring (Figure S5, Supporting Information). In Model S2, S atom adopts sp^2-hybridization featuring three in-plane hybridized orbitals and one perpendicular p_z orbital. The three in-plane hybridized orbitals of S atom form two covalent bonds with adjacent carbon atoms (Figure 2b) and accommodate a lone pair (Figure 2c). C3 atom also adopts sp^2-hybridization possessing two covalent bonds and a lone pair. The p_z orbitals of S and C3 atom form a π bond, which replaces the carbon-carbon triple bond in pristine graphdiyne (Figure 2d). Model S2 is energetically more favorable than Models S1 or S3, because the lone pair of S can be stabilized by aromatic benzene ring and the lone pair of C3 atom can be stabilized by the resonance with the neighboring carbon–carbon triple bond. The planar structure of Model S3 is attributed to the interaction between the lone pair of S atom and the vacant p_z orbital of the carbon atom close to the hexagonal ring (Figure S6, Supporting Information).

The strong stabilizing effects induced by the aromatic benzene ring and the carbon–carbon triple bond also hold true in Models N2 and P2: the lowest-energy configurations for the N- and P-doped graphdiynes. In contrast to S-doped graphdiynes, N- and P-doped graphdiynes have unpaired electrons on carbon

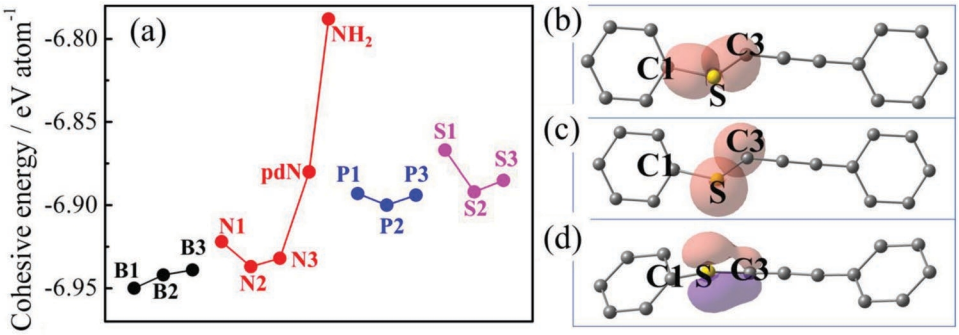

Figure 2. a) The cohesive energies of X-doped graphdiynes. b–d) Selected NBO orbitals of Model S2 with an isovalue of 0.08, where S and C3 are sp^2 hybridized. The hexagonal rings are passivated by H atoms, which are invisible in the plots.

atoms and lone pair electrons on N/P atoms (Figures S7–S12, Supporting Information). Based on our NBO analysis, the aromaticity of the hexagonal carbon ring is broken by the lone pair on the N/P atom in Model N1/P1 (Figures S7 and S10, Supporting Information), which makes N1/P1 energetically less favorable. For Model N2/P2, the lone pair on N/P can be stabilized by the hexagonal ring adjacent to the N dopant, moreover, the unpaired electron located on the C3 atom can resonate to the C5 atom, and then conjugate with its neighboring hexagonal ring (Figure S8d, Supporting Information). These two effects help stabilize N2/P2 over N3/P3. The planar structure of P3 is attributed to the sp^2 hybridization of the P atom and the π bond between P and the C2 atom (Figure S12, Supporting Information).

On the contrary, for B-doped graphdiynes, Model B1 is lower in energy than B2 or B3, which can be explained by the relatively good π-electron delocalization in the BC$_5$H ring[62] and the strong π conjugation through the vacant p orbital of the B atom.

3.2. The Mechanism of ORR/OER

The direct four-electron pathway of ORR is preferred for fuel cells and metal–air batteries, as it provides high voltage and produces minimum harmful peroxides. In acidic condition, this pathway has four reaction steps

$$O_2(g) + H^+ + e^- + * = *OOH \quad (2a)$$

$$*OOH + H^+ + e^- = *O + H_2O(l) \quad (2b)$$

$$*O + H^+ + e^- = *OH \quad (2c)$$

$$*OH + H^+ + e^- = * + H_2O(l) \quad (2d)$$

where * denotes the active site, *OOH, *O, and *OH represent the oxygen-containing intermediates. The reaction free energy change for each step can be derived by free adsorption energies as[63]

$$\Delta G(2a) = \Delta G(*OOH) - 4.92\,eV + eU_a \quad (3a)$$

$$\Delta G(2b) = \Delta G(*O) - \Delta G(*OOH) + eU_b \quad (3b)$$

$$\Delta G(2c) = \Delta G(*OH) - \Delta G(*O) + eU_c \quad (3c)$$

$$\Delta G(2d) = \Delta G(*OH) + eU_d \quad (3d)$$

where the term U_i (i = a, b, c, d) is the external potential on the electrode. The four-electron mechanism for OER is given in Supporting Information due to its similarity to ORR.

3.3. Active Sites, Scaling Relations, and Volcano Plots

The dopants themselves and the carbon atoms with high spin and/or charge density (Figures S13–S24, Supporting Information) were chosen as possible active sites.[64–66] These possible active sites are labeled by combining the heteroatom doping model and the doping position as numbered in Model Gdy. For example, the active site N3-C4 is the C atom numbered 4 in Model N3.

Based on the free adsorption energies of oxygen-containing species on these active sites (Table S1, Supporting Information), we plotted the scaling relations (**Figure 3**a), which depict the correlation of ΔG(*OOH), ΔG(*O) and ΔG(*OH) at each possible active site

$$\Delta G(*OOH) = 0.89\ \ \Delta G(*OH) + 3.30 \quad (4a)$$

$$\Delta G(*O) = 1.18\ \ \Delta G(*OH) + 0.68 \quad (4b)$$

Substituting Equation (4) to Equation (3), and letting ΔG(2i) = 0 (i = a–d), we obtained the reversible potentials U_i^0

$$eU_a^0 = -0.89\,\Delta G(*OH) + 1.62 \quad (5a)$$

$$eU_b^0 = -0.29\,\Delta G(*OH) + 2.62 \quad (5b)$$

$$eU_c^0 = 0.18\,\Delta G(*OH) + 0.68 \quad (5c)$$

$$eU_d^0 = \Delta G(*OH) \quad (5d)$$

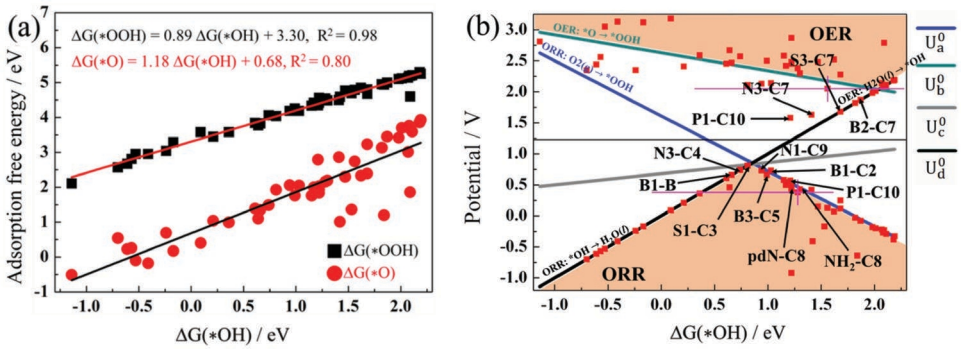

Figure 3. a) The scaling relations between the free adsorption energies of O-containing intermediates. b) The volcano plot of limiting potentials for X-doped graphdiynes toward ORR/OER. The best ORR/OER active sites in Model Gdy are denoted by magenta crosses, while the active sites with catalytic performance better than that of Model Gdy are labeled by arrows.

Based on these reversible potentials, we constructed the volcano plots for X-doped graphdiynes to screen possible active sites. As shown in Figure 3b, the reversible potentials U_i^0 form two volcanos (orange areas): ORR at the bottom, and OER at the top. Theoretically, the limiting potential (U_L) is the maximum/minimum potential that allows ORR/OER. Its value for each active site is marked by a red square in the volcano plots. Overall, the ORR volcano is slightly inclined to the left compared to the OER volcano, indicating that the best active sites for ORR and OER are different in X-doped graphdiynes. For ORR, there are two rate-determining steps (RDS): one is the fourth reaction step (the reduction of *OH to H_2O(l), Equation 2d) with strong *OH adsorption, and the other is the first reaction step (the formation of *OOH species, Equation 2a) with weak *OH adsorption. For OER, there are also two rate-determining steps: one is the third reaction step (the oxidation of *O to *OOH species, Equation S1c, Supporting Information) with strong *OH adsorption, and the other is the first reaction step (the oxidation of H_2O to *OH species, Equation S1a, Supporting Information) with weak *OH adsorption.

3.4. Evaluations of Catalytic Performances

Heteroatom (N, B, P, and S) doping can enhance the ORR activities of graphdiynes. Among the heteroatom-doped graphdiynes examined in this study, the graphitic S-doped graphdiyne has the best ORR performance with the nearby C3 atom as the active site (S1-C3, Figure 1m). For N-doped graphdiynes, the sp-N-doped graphdiyne (Model N3) exhibits the best catalytic performance, whose active site is the carbon atom C4 adjacent to the N dopant (N3-C4, Figure 1d). The graphitic B-doped graphdiyne shows comparable performance to that of sp-N-doped graphdiyne, with the neighboring C2 atom as the active site (B1-C2, Figure 1g). Compared with the pristine graphdiyne, the graphitic P-doped graphdiyne displays improved activity, whose active site is C10 at the opposite site of P dopant in the hexagonal ring (P1-C10, Figure 1j).

Two ORR catalysts show comparable or even better limiting potentials than that of a Pt (111) surface (U_L = 0.79 V),[67] namely the sp-N-doped graphdiyne (active site: N3-C4, U_L = 0.74 V) and the graphitic S-doped graphdiyne (active site: S1-C3, U_L = 0.81 V). Their high ORR activities are attributed to large positive charges on the corresponding active sites (**Figure 4**a,c): The net charge of N3-C4 (ca. 0.06 |e|) the second largest in Model N3 (only smaller than that of C2, Figure S19a, Supporting Information), while the net charge of S1-C3 is the largest (about 0.03 |e|) among all the carbon atoms in Model S1 (Figure S23, Supporting Information).

Then, we utilized the free energy diagrams to evaluate the catalytic performance of the active sites N3-C4 and S1-C3 under various potentials (Figure 4b,d). At the equilibrium potential (1.23 V), three ORR reaction steps are uphill on both N3-C4 and S1-C3 active sites, which means that ORR cannot occur spontaneously at this condition. The four ORR reaction steps are all downhill on these two active sites by tuning the potential to 0 V, which corresponds to a short circuit condition of fuel cell. The maximum potentials that allow ORR spontaneously, i.e., the limiting potentials, on N3-C4 and S1-C3 are 0.74 and 0.81 V, respectively. Thus, the overpotential (η) on N3-C4 is 0.49 V, and η on S1-C3 is 0.42 V.

Heteroatom (N, B, P, and S) doping also promotes the OER activities of graphdiynes. Among all the doped graphdiynes, the graphitic P-doped system exhibits the best OER activity, and its corresponding active site (P1-C10, Figure 1j) is also active for ORR. The sp-N-doped graphdiyne (Model N3) can serve as a bifunctional catalyst, being able to well catalyze both ORR and OER at the same active site (N3-C7, Figure 1d). Compared with the pristine graphdiyne, sp-B- and sp-S-doped graphdiynes also have enhanced OER activities, with active sites at B2-C7 (Figure 1h) and S3-C7 (Figure 1o), respectively.

RuO_2 is generally regarded as the best OER electrocatalyst,[68,69] whose theoretical limiting potential is about 1.60 V.[70] In terms of the limiting potential, two catalysts examined here have comparable or even better OER activity than RuO_2: the sp-N-doped graphdiyne (active site: N3-C7, U_L = 1.63 V), and the graphitic P-doped graphdiyne (active site: P1-C10, U_L = 1.58 V). The high OER activities are attributed to the high spin on the corresponding active sites (**Figure 5**a,c). N3-C7 has a moderate positive charge, but a very high spin of 0.04 μ_B, which is only smaller than that of C2 atom in the same model (Figure S19, Supporting Information); while P1-C10 not only

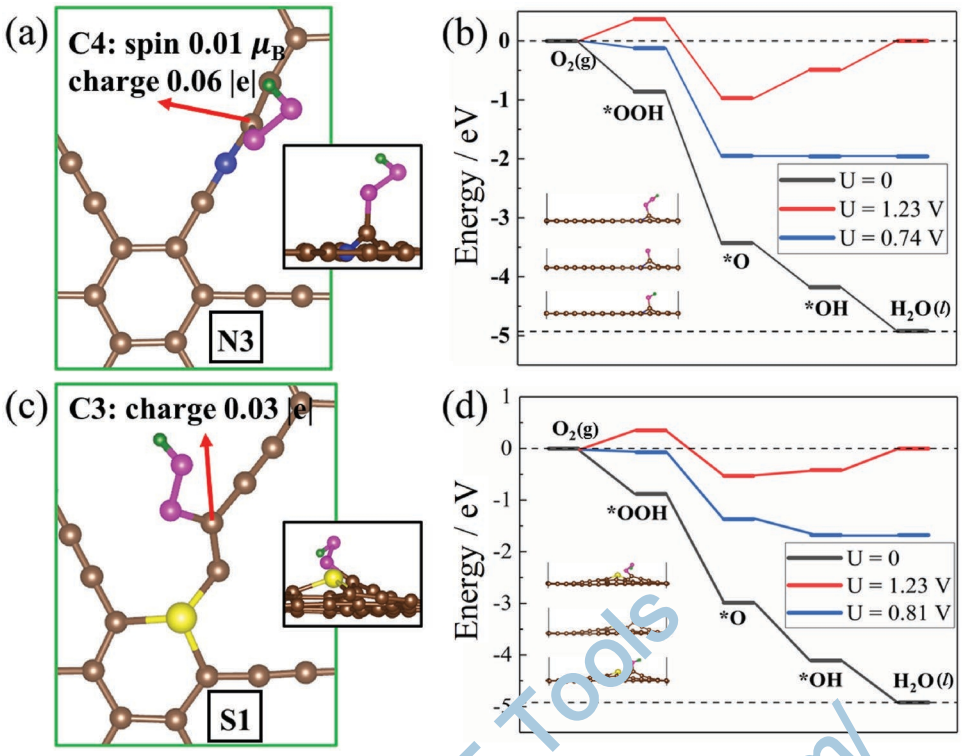

Figure 4. The scheme of *OOH intermediate adsorbed on ORR active sites N3-C4 a) and S1-C3 c). The energy diagram for ORR under various potentials on active site on N3-C4 b) and S1-C3 d).

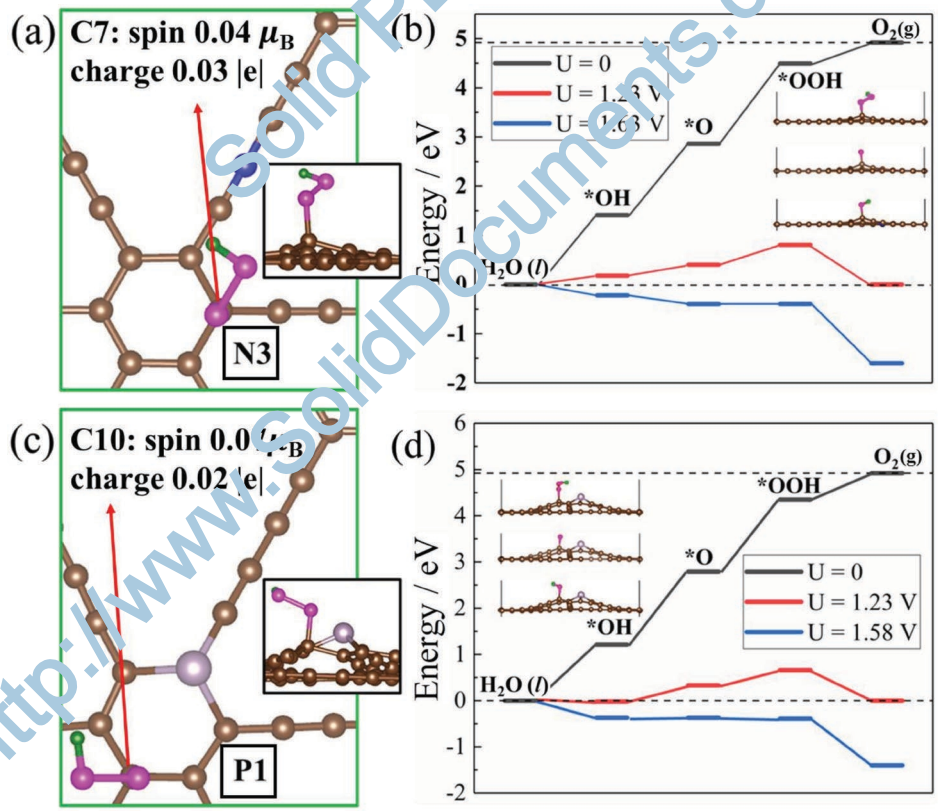

Figure 5. The scheme of *OOH intermediate adsorbed on OER active site N3-C7 a) and P1-C10 c). The Gibbs free energy diagram for OER under various potentials on the active site N3-C7 b) and P1-C10 d).

has a high positive charge, but also a very high spin of 0.07 μ_B (Figure S20, Supporting Information).

Figure 5b,d presents the OER Gibbs energy diagrams on the N3-C7 and P1-C10 active sites for the sp-N-doped graphdiyne and the graphitic P-doped graphdiyne. At 0 or 1.23 V, N3-C7 or P1-C10 cannot catalyze OER because of uphill reaction steps. Increasing the external potential from zero on the electrode could make the uphill OER reaction steps become downhill. The minimum potential that allows OER, or the limiting potential, is 1.63 V for N3-C7, while the corresponding value is 1.58 V for P1-C10. Thus, the OER overpotential for N3-C7 and P1-C10 are 0.40 and 0.35 V, respectively.

Zhang et al. heat-treated the graphdiyne with ball-milled sulfur to obtain the S-doped graphdiyne, which was proven to exhibit a ferromagnetic transition temperature of about 460 K.[71] Yang et al. heated the graphdiyne with benzyl disulfides, and the as-prepared S-doped graphdiyne behaves better than the pristine graphdiyne as the electrode for Li-ion battery.[72] Zhao et al. synthesized N, S codoped graphdiyne (NSFLGDY) by calcining few-layer graphdiyne oxides with melamine and dibenzyl sulfide and confirmed the superior OER activity of NSFLGDY, which is even better than RuO_2.[73]

4. Conclusions

In the present work, we explored the ORR/OER electrocatalytic activities of N-, B-, P-, and S-doped graphdiynes systematically by means of DFT computations. Our calculations revealed that the sp-N-doped graphdiyne (–C≡N–C≡C–), the graphitic P-doped and the graphitic P-doped graphdiynes exhibit comparable or even better catalytic activities compared with Pt/C or RuO_2. The sp-N dopant is the most crucial dopant for N-doped graphdiynes, as it can generate not only an ORR active site (C3 in Model N3, $\eta = 0.49$ V), but also an OER active site (C7 in Model N3, $\eta = 0.40$ V). The graphitic doping type of S atom endows graphdiyne the best ORR catalytic performance ($\eta = 0.42$ V) on the active site labeled as C3 in Model S1. And the graphitic doping type of P atom grants graphdiyne the best OER catalytic performance ($\eta = 0.35$ V) on the active site labeled as C10 in Model P1. The high ORR activities (at C3 in Models N3 and S1) are attributed to the large positive charge, while the high spin densities are responsible for the high OER activities (at C7 in Model N3 and C10 in Models P1). Overall, this work illustrates the underlying mechanism of the high ORR activity of the sp-N-doped graphdiyne and demonstrates its efficacy as an OER catalyst. This work also unveils the promise of S- and P-doped graphdiynes as ORR and OER catalysts, respectively, which guides the further design of effective ORR/OER electrocatalysts.

Supporting Information

Supporting Information is available from the Wiley Online Library or from the author.

Acknowledgements

This work was supported by the National Science Foundation-Centers of Research Excellence in Science and Technology (NSF-CREST Center) for Innovation, Research and Education in Environmental Nanotechnology (CIRE2N) (Grant No. HRD-1736093), and FIPI fund of University of Puerto Rico. The authors thank Josué A. Benjamín Rivera, Daniel Ramos Pérez, Shiru Lin, and Long Zhou for critical reading, comments, and suggestions in the "Advanced Scientific Writing" course. The authors benefited significantly from "Writing in the Sciences," given by Professor Kristin L. Sainani, an online course authorized by Stanford University and offered through Coursera. This research used resources of the High Performance of Computational facility (HPCf), University of Puerto Rico, which is partially supported by an Institutional Development Award (IDeA) INBRE Grant Number P20GM103475 from the National Institute of General Medical Sciences (NIGMS), a component of the National Institutes of Health (NIH), and the Bioinformatics Research Core of the INBRE. Its contents are solely the responsibility of the authors and do not necessarily represent the official view of NIH.

Conflict of Interest

The authors declare no conflict of interest.

Keywords

density functional calculations, heteroatom-doped graphdiynes, metal-free electrocatalysts, oxygen evolution reaction, oxygen reduction reaction

Received: December 28, 2018
Revised: March 7, 2019
Published online:

[1] L. Carrette, K. Friedrich, U. Stimming, *Fuel cells* **2001**, *1*, 5.
[2] G. J. Acres, *J. Power Sources* **2001**, *100*, 60.
[3] Y. Li, J. Lu, *ACS Energy Lett.* **2017**, *2*, 1370.
[4] H. F. Wang, C. Tang, Q. Zhang, *Adv. Funct. Mater.* **2018**, *28*, 1803329.
[5] Y. Wang, H. Suzuki, J. Xie, O. Tomita, D. J. Martin, M. Higashi, D. Kong, R. Abe, J. Tang, *Chem. Rev.* **2018**, *118*, 5201.
[6] D. Kang, T. W. Kim, S. R. Kubota, A. C. Cardiel, H. G. Cha, K.-S. Choi, *Chem. Rev.* **2015**, *115*, 12839.
[7] Z. P. Cano, D. Banham, S. Ye, A. Hintennach, J. Lu, M. Fowler, Z. Chen, *Nat. Energy* **2018**, *3*, 279.
[8] Y. Lee, J. Suntivich, K. J. May, E. E. Perry, Y. Shao-Horn, *J. Phys. Chem. Lett.* **2012**, *3*, 399.
[9] P. J. Ferreira, G. J. la O', Y. Shao-Horn, D. Morgan, R. Makharia, S. Kocha, H. A. Gasteiger, *J. Electrochem. Soc.* **2005**, *152*, A2256.
[10] M. Winter, R. J. Brodd, *Chem. Rev.* **2004**, *104*, 4245.
[11] Y. Bing, H. Liu, L. Zhang, D. Ghosh, J. Zhang, *Chem. Soc. Rev.* **2010**, *39*, 2184.
[12] Z. Li, D. Wang, Y. Wu, Y. Li, *Natl. Sci. Rev.* **2018**, *5*, 673.
[13] J. Wang, Z. Li, Y. Wu, Y. Li, *Adv. Mater.* **2018**, *30*, 1801649.
[14] X. Wang, W. Wang, M. Qiao, G. Wu, W. Chen, T. Yuan, Q. Xu, M. Chen, Y. Zhang, X. Wang, *Sci. Bull.* **2018**, *63*, 1246.
[15] Z. Chen, D. Higgins, A. Yu, L. Zhang, J. Zhang, *Energy Environ. Sci.* **2011**, *4*, 3167.
[16] F. Jaouen, E. Proietti, M. Lefèvre, R. Chenitz, J.-P. Dodelet, G. Wu, H. T. Chung, C. M. Johnston, P. Zelenay, *Energy Environ. Sci.* **2011**, *4*, 114.
[17] J. Yang, Z. Qiu, C. Zhao, W. Wei, W. Chen, Z. Li, Y. Qu, J. Dong, J. Luo, Z. Li, Y. Wu, *Angew. Chem., Int. Ed. Engl.* **2018**, *57*, 14095.
[18] Y. Qu, Z. Li, W. Chen, Y. Lin, T. Yuan, Z. Yang, C. Zhao, J. Wang, C. Zhao, X. Wang, *Nat. Catal.* **2018**, *1*, 781.
[19] L. Dai, Y. Xue, L. Qu, H.-J. Choi, J.-B. Baek, *Chem. Rev.* **2015**, *115*, 4823.

[20] D. Yu, Q. Zhang, L. Dai, *J. Am. Chem. Soc.* **2010**, *132*, 15127.
[21] D. Yu, E. Nagelli, F. Du, L. Dai, *J. Phys. Chem. Lett.* **2010**, *1*, 2165.
[22] X. Lepró, R. Ovalle-Robles, M. D. Lima, A. L. Elías, M. Terrones, R. H. Baughman, *Adv. Funct. Mater.* **2012**, *22*, 1069.
[23] K. Gong, F. Du, Z. Xia, M. Durstock, L. Dai, *Science* **2009**, *323*, 760.
[24] H. Zhang, X. Li, X. Meng, S. Zhou, G. Yang, X. Zhou, *J. Phys.: Condens. Matter* **2019**, *31*, 125301.
[25] K. S. Novoselov, A. K. Geim, S. V. Morozov, D. Jiang, Y. Zhang, S. V. Dubonos, I. V. Grigorieva, A. A. Firsov, *Science* **2004**, *306*, 666.
[26] Z.-H. Sheng, H.-L. Gao, W.-J. Bao, F.-B. Wang, X.-H. Xia, *J. Mater. Chem.* **2012**, *22*, 390.
[27] Z. Yang, Z. Yao, G. Li, G. Fang, H. Nie, Z. Liu, X. Zhou, X. Chen, S. Huang, *ACS Nano* **2011**, *6*, 205.
[28] J. P. Paraknowitsch, A. Thomas, *Energy Environ. Sci.* **2013**, *6*, 2839.
[29] M. Liu, R. Zhang, W. Chen, *Chem. Rev.* **2014**, *114*, 5117.
[30] L. Qu, Y. Liu, J.-B. Baek, L. Dai, *ACS Nano* **2010**, *4*, 1321.
[31] H. B. Yang, J. Miao, S.-F. Hung, J. Chen, H. B. Tao, X. Wang, L. Zhang, R. Chen, J. Gao, H. M. Chen, *Sci. Adv.* **2016**, *2*, e1501122.
[32] H. Jiang, J. Gu, X. Zheng, M. Liu, X. Qiu, L. Wang, W. Li, Z. Chen, X. Ji, J. Li, *Energy Environ. Sci.* **2019**, *12*, 322.
[33] R. Jain, R. Narayan, S. P. Sasikala, K. E. Lee, H. J. Jung, S. O. Kim, *2D Mater.* **2017**, *4*, 042006.
[34] R. Gusmão, Z. Sofer, D. Bouša, M. Pumera, *Angew. Chem., Int. Ed. Engl.* **2017**, *56*, 14417.
[35] J. Zhang, Y. Chen, X. Wang, *Energy Environ. Sci.* **2015**, *8*, 3092.
[36] Z. Pei, J. Gu, Y. Wang, Z. Tang, Z. Liu, Y. Huang, Y. Huang, J. Zhao, Z. Chen, C. Zhi, *ACS Nano* **2017**, *11*, 6004.
[37] G. Li, Y. Li, H. Liu, Y. Guo, Y. Li, D. Zhu, *Chem. Commun.* **2010**, *46*, 3256.
[38] M. Long, L. Tang, D. Wang, Y. Li, Z. Shuai, *ACS Nano* **2011**, *5*, 2593.
[39] C. Huang, Y. Li, N. Wang, Y. Xue, Z. Zuo, H. Liu, Y. Li, *Chem. Rev.* **2018**, *118*, 7744.
[40] H. Shang, Z. Zuo, H. Zheng, K. Li, Z. Tu, Y. Yi, H. Liu, Y. Li, *Nano Energy* **2018**, *44*, 144.
[41] Y. Li, C. Guo, J. Li, W. Liao, Z. Li, J. Zhang, C. Chen, *Carbon* **2017**, *119*, 201.
[42] W. Si, Z. Yang, X. Wang, Q. Lv, F. Zhao, X. Li, [illegible], Y. Long, J. Gao, C. Huang, *ChemSusChem* **2019**, *12*, 173[illegible].
[43] R. Liu, H. Liu, Y. Li, Y. Yi, X. Shang, S. Zhang, X. Yu, S. Zhang, H. Cao, G. Zhang, *Nanoscale* **2014**, *6*, 11336.
[44] Q. Lv, W. Si, Z. Yang, N. Wang, Z. Tu, Y. Yi, C. Huang, L. Jiang, M. Zhang, J. He, Y. Long, *ACS Appl. Mater. Interfaces* **2017**, *9*, 29744.
[45] Q. Lv, W. Si, J. He, L. Sun, C. Zhang, N. Wang, Z. Yang, X. Li, X. Wang, W. Deng, Y. Long, C. Huang, Y. Li, *Nat. Commun.* **2018**, *9*, 3376.
[46] Y. Zhao, J. Wan, H. Yao, L. Zhang, K. Lin, L. Wang, N. Yang, D. Liu, L. Song, J. Zhu, L. Gu, L. Liu, H. Zhao, Y. Li, D. Wang, *Nat. Chem.* **2018**, *10*, 924.
[47] W. Sun, S. X. Dou, *Chem* **2018**, *4*, 2024.
[48] S. Zhang, Y. Cai, H. He, Y. Zhang, R. Liu, H. Cao, M. Wang, J. Liu, G. Zhang, Y. Li, H. Liu, B. Li, *J. Mater. Chem. A* **2016**, *4*, 4738.
[49] B. K. Das, D. Sen, K. K. Chattopadhyay, *Phys. Chem. Chem. Phys.* **2016**, *18*, 2949.
[50] N. Ketabi, T. M. Tolhurst, B. Leedahl, H. Liu, Y. Li, A. Moewes, *Carbon* **2017**, *123*, 1.
[51] B. K. Das, D. Sen, K. K. Chattopadhyay, *Carbon* **2016**, *105*, 330.
[52] B. Delley, *J. Chem. Phys.* **2000**, *113*, 7756.
[53] J. P. Perdew, K. Burke, M. Ernzerhof, *Phys. Rev. Lett.* **1996**, *77*, 3865.
[54] S. Grimme, *J. Comput. Chem.* **2006**, *27*, 1787.
[55] A. Klamt, G. Schüürmann, *J. Chem. Soc., Perkin Trans. 2* **1993**, 799.
[56] B. Delley, *J. Chem. Phys.* **1990**, *92*, 508.
[57] H. J. Monkhorst, J. D. Pack, *Phys. Rev. B* **1976**, *13*, 5188.
[58] F. L. Hirshfeld, *Theor. Chim. Acta* **1977**, *44*, 129.
[59] a) J. K. Nørskov, J. Rossmeisl, A. Logadottir, L. Lindqvist, J. R. Kitchin, T. Bligaard, H. Jonsson, *J. Phys. Chem. B* **2004**, *108*, 17886; b) J. Rossmeisl, A. Logadottir, J. K. Nørskov, *Chem. Phys.* **2005**, *319*, 178.
[60] X. Wang, G. Sun, P. Routh, D.-H. Kim, W. Huang, P. Chen, *Chem. Soc. Rev.* **2014**, *43*, 7067.
[61] a) M. J. Frisch, G. W. Trucks, H. B. Schlegel, G. E. Scuseria, M. A. Robb, J. R. Cheeseman, G. Scalmani, V. Barone, B. Mennucci, G. A. Petersson, H. Nakatsuji, M. Caricato, X. Li, H. P. Hratchian, A. F. Izmaylov, J. Bloino, G. Zheng, J. L. Sonnenberg, M. Hada, M. Ehara, K. Toyota, R. Fukuda, J. Hasegawa, M. Ishida, T. Nakajima, Y. Honda, O. Kitao, H. Nakai, T. Vreven, J. A. Montgomery Jr., J. E. Peralta, F. Ogliaro, M. Bearpark, J. J. Heyd, E. Brothers, K. N. Kudin, V. N. Staroverov, T. Keith, R. Kobayashi, J. Normand, K. Raghavachari, A. Rendell, J. C. Burant, S. S. Iyengar, J. Tomasi, M. Cossi, N. Rega, J. M. Millam, M. Klene, J. E. Knox, J. B. Cross, V. Bakken, C. Adamo, J. Jaramillo, R. Gomperts, R. E. Stratmann, O. Yazyev, A. J. Austin, R. Cammi, C. Pomelli, J. W. Ochterski, R. L. Martin, K. Morokuma, V. G. Zakrzewski, G. A. Voth, P. Salvador, J. J. Dannenberg, S. Dapprich, A. D. Daniels, O. Farkas, J. B. Foresman, J. V. Ortiz, J. Cioslowski, D. J. Fox, Gaussian 09, Revision B.01, Gaussian, Inc., Wallingford, CT **2010**; b) E. D. Glendening, A. E. Reed, J. E. Carpenter, F. Weinhold, NBO Version 3.1., http://gaussian.com/nbo3.1/.
[62] S. Giri, B. Z. Chada, P. Jena, *ChemPhysChem* **2014**, *15*, 2903.
[63] W. Liang, J. Chen, Y. Liu, S. Chen, *ACS Catal.* **2014**, *4*, 4170.
[64] L. Zhang, Z. Xia, *J. Phys. Chem. C* **2011**, *115*, 11170.
[65] M. Li, Y. Zhang, Q. Xu, J. Niu, Z. Xia, *J. Catal.* **2014**, *314*, 66.
[66] [illegible] W. Wang, L. Zhang, Z. Xia, A. Roy, D. W. Chang, J. B. Baek, L. Dai, *Angew. Chem. Int. Ed. Engl.* **2012**, *51*, 4209.
[67] V. Tripković, E. Skúlason, S. Siahrostami, J. K. Nørskov, J. Rossmeisl, *Electrochim. Acta* **2010**, *55*, 7975.
[68] E. Fabbri, A. Habereder, K. Waltar, R. Kötz, T. J. Schmidt, *Catal. Sci. Technol.* **2014**, *4*, 3800.
[69] I. C. Man, H. Y. Su, F. Calle-Vallejo, H. A. Hansen, J. I. Martínez, N. G. Inoglu, J. Kitchin, T. F. Jaramillo, J. K. Nørskov, J. Rossmeisl, *ChemCatChem* **2011**, *3*, 1159.
[70] J. Rossmeisl, Z.-W. Qu, H. Zhu, G.-J. Kroes, J. K. Nørskov, *J. Electroanal. Chem.* **2007**, *607*, 83.
[71] M. Zhang, H. Sun, X. Wang, H. Du, J. He, Y. Long, Y. Zhang, C. Huang, *J. Phys. Chem. C* **2019**, *123*, 5010.
[72] Z. Yang, W. Cui, K. Wang, Y. Song, F. Zhao, N. Wang, Y. Long, H. Wang, C. Huang, *Chem. Eur. J.* **2019**, *25*, 5643.
[73] Y. Zhao, N. Yang, H. Yao, D. Liu, L. Song, J. Zhu, S. Li, L. Gu, K. Lin, D. Wang, *J. Amer. Chem. Soc.* **2019**, *141*, 7240.